Birefringent Anti-resonant Hollow-core Fiber

Stephanos Yerolatsitis, Riley Shurvinton, Peng Song, Yaping Zhang, Robert J. A. Francis-Jones, Kristina R. Rusimova

***Abstract*— Hollow-core fibers have demonstrated record performance in applications such as high-power pulse delivery, quantum computing, and sensing. However, their routine use is yet to become reality. A major obstacle is the ability to maintain the polarization state of light over a broad range of wavelengths, while also ensuring single-mode guidance and attenuation that is low enough for practical applications that require only a few meters of fiber length (<1 dB/m). Here we simulated, fabricated and characterized a single-mode birefringent anti-resonant hollow-core fiber. The birefringence was achieved by introducing capillary tubes of different thicknesses, thereby creating reduced symmetry in the structure. The measured group birefringence is in good agreement with the calculated group birefringence from simulations across the fiber guidance band within the telecommunications C-band. At 1550 nm, we measured a group birefringence of 4.4×10^{-5}, which corresponds to a phase birefringence of 2.5×10^{-5}. The measured loss of the fiber was 0.46 dB/m at 1550 nm. The measured polarization extinction ratio of the fiber at 1550 nm was 23.1 dB (25.7 dB) along the x-(y-) polarization axis, relating to an h-parameter of 9.8×10^{-4} (5.3×10^{-4}).**

***Index Terms*— Birefringence, Optical fiber fabrication, Optical fibers**

I. Introduction

Air-guidance in hollow-core fibers holds the key to many exciting possibilities, e.g. high-energy pulse delivery [1], [2], deep-UV [3] and mid-IR [4] guidance, gas spectroscopy and gas lasers [5], [6], precise interferometric sensing [7], as well as the possibility for the lowest loss signal transmission [8], [9], [10]. However, their widespread practical use in many applications is hampered by the need to further understand the guiding mechanism of hollow-core fibers, for example how to maintain the polarization state of the guided light. In solid core fibers, polarization control is achieved either by introducing stress rods in the cladding structure, or by forming shape anisotropy (e.g. by increasing the ellipticity of the core) [11]. Nevertheless, due to the inherent material properties of traditional silica fibers, their use has its limitations – namely, low damage threshold, material dispersion, and absorption. Hollow-core fibers offer a practical route to overcoming these limitations. However, in hollow-core fibers, light is confined within an air-core and therefore there is very little interaction with the dispersive silica cladding material. In addition, it is difficult to induce modal birefringence in these fibers with the methods applied to traditional solid-core fibers. Previously, high birefringence was demonstrated in hollow-core photonic bandgap fibers (HC-PBGF) by fabricating an elliptical core [12] or by modifying the cladding structure of the fiber to introduce polarization dependent loss [13]. Although HC-PBGFs have solved some of the issues associated with standard step-index fibers, they are complicated to fabricate, and have a narrow operating bandwidth.

Resurgent interest in hollow-core fibers has resulted in the development of anti-resonant hollow-core fibers [14]–[16]. The guiding mechanism in anti-resonant fibers is much simpler compared to that in photonic-bandgap fibers. The cladding structure of anti-resonant fibers comprises a ring of capillary tubes surrounding an air core. The walls of these capillaries act as Fabry-Perot resonators, confining the light in the core at their anti-resonant wavelengths. Numerical simulations of various anti-resonant structures have revealed the possibility of achieving shape birefringence in such fibers [17]–[20], but their practical demonstration remains elusive mainly because of the complexity of the design which increases the difficulty of the fabrication of the fiber. Here, we report in detail the first fabrication and characterization of a birefringent anti-resonant hollow-core fiber.

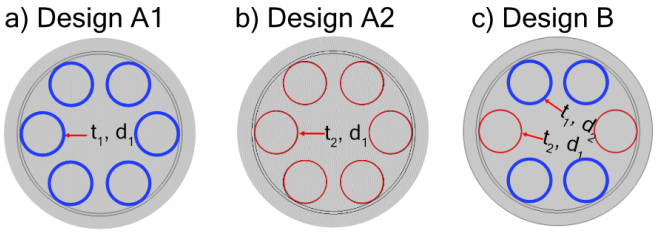

Fig. 1. Schematic diagram of the fiber designs (a) A1, (b) A2, and (c) B, with corresponding capillary tube thicknesses t_1 and t_2, and capillary tube diameters d_1 and d_2.

II. Simulated Designs and Fiber Fabrication

Standard anti-resonant hollow-core fibers consist of a ring of capillary tubes around a hollow core, with all capillary tubes of the same diameter and thickness. Figure 1 and Table 1 introduce

S. Yerolatsitis and K. R. Rusimova are with the Centre for Photonics and Photonic Materials, University of Bath, Bath BA2 7AY and the Department of Physics, University of Bath, Bath, BA2 7AY, UK (Corresponding authors: s.yerolatsitis@bath.ac.uk; k.r.rusimova@bath.ac.uk)

R. Shurvinton is with the Department of Physics, University of Bath, Bath, BA2 7AY, UK

P. Song and Y. Zhang are with the School of Physics and Technology, University of Jinan, Jinan, 250022, Shandong, China

R. J. A. Francis-Jones was with the Centre for Photonics and Photonic Materials, University of Bath, Bath BA2 7AY, UK and is now with the Clarendon Laboratory, University of Oxford, Parks Road, Oxford, OX1 3PU, UK

the parameters of the three fiber designs that we compare. Designs A1 and A2 are standard anti-resonant hollow-core fibers with respective tube thicknesses t_1 and t_2, and the same tube diameter d_1. In our birefringent hollow-core fiber, design B, the modal birefringence is achieved by changing the thickness t_2 of two capillary tubes, and thereby reducing the rotational symmetry in the structure below threefold while maintaining the simplicity of the design by using a single ring of tubes. We believe that doing so introduces form birefringence due to the guided modes interacting differently with different parts of the structure.

TABLE I
PARAMETERS OF THE ANTI-RESONANT HOLLOW-CORE FIBER DESIGNS.

Design	A1	A2	B
Core diameter (μm)	26	26	26
Thickness, t_1 (nm)	610	-	610
Thickness, t_2 (nm)	-	210	210
Capillary tube diameter, d_1 (μm)	16.1	16.1	16.1
Capillary tube diameter, d_2 (μm)	-	-	16.7

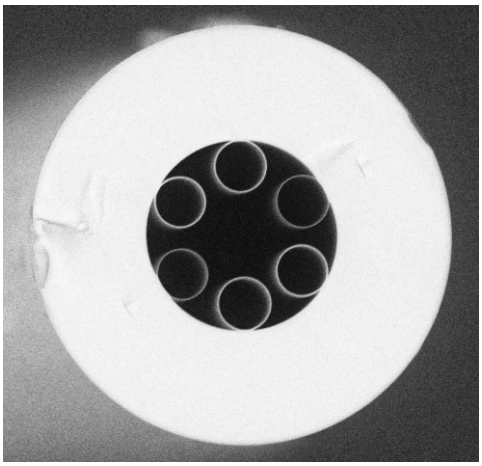

Fig. 2. Cross-sectional SEM (scanning electron microscope) image of the birefringent hollow-core fiber. The outer diameter of the fiber is 125 μm and the core diameter is 26 μm. The capillary tube wall thicknesses are $t_1 = 610$ nm and $t_2 = 210$ nm.

Figure 2 shows a scanning electron microscope image of the hollow-core fiber fabricated based on design B using the stack-and-draw method. All six capillary tubes have a similar outer diameter (~16 μm). A small variation in the diameter between the two sets of capillary tubes of different thicknesses is due to the differential pressurization technique used to fabricate the fiber. Two of the capillary tubes (opposite to each other, across the axis of the fiber) are three times thinner ($t_2 = 210$ nm) compared to the other four ($t_1 = 610$ nm). According to the anti-resonant reflecting optical waveguide (ARROW) model, the four thicker capillary tubes will have their first resonance at around 1280 nm, and their second resonance at 640 nm, whereas the two thinner capillary tubes will have their first resonance at around 440 nm [14]. The outer diameter of the fiber is 125 μm and the core diameter is 26 μm. In order to increase the interaction of the guided mode with the surrounding glass structure, the core size was intentionally selected such that it is half the size that typically ensures minimal attenuation at 1550 nm [21], [22]. The capillary tube diameter to core diameter ratio was selected to ensure single mode operation of the fiber [23].

Using the parameters in Table 1 and a finite element method solver (COMSOL Multiphysics 5.3a), we simulated all three fiber designs and obtained the effective refractive index of the fundamental mode in the two orthogonal polarizations (n_x and n_y) across a range of wavelengths. By using large mesh densities ($\lambda/6$ in the glass regions) across the structure, the calculations were performed with the same degree of confidence as in reference [22]. Figure 3(a-c) shows a schematic diagram of each of the fiber designs from Table 1, together with their corresponding confinement loss as a function of wavelength. As per the ARROW model, design A1 has a guidance band at wavelengths above its first resonance at 1280 nm (shaded in blue), and a second guidance band between its first resonance and its second resonance at 640 nm (shaded in red). On the other hand, design A2 has its first resonance at 440 nm and an associated guidance band at wavelengths above this resonance (shaded in blue). Far from this first resonance, above 1700 nm, the confinement loss increases very rapidly, setting the upper bound of the anti-resonant guidance band. Design B, which combines tube thicknesses from both designs A1 and A2, has two anti-resonant guidance bands, similar to design A1. Note, both shaded regions (red and blue) highlight guidance where the confinement loss is lower than 2 dB/m in design B. The lowest calculated confinement loss of design B in each guidance band is the same as that of the other two designs at those wavelengths, with ≈ 0.01 dB/m at 780 nm (close to the performance of single ring anti-resonant hollow-core fibers [8], [22]), and ≈ 0.75 dB/m at 1550 nm. It is important to note the difference in the width of the longer wavelength transmission band (in blue) between designs A1 and B. The much narrower guidance band for design B is bound by the first resonance of design A1 at one end (lower wavelength edge of shaded blue region in Fig. 3(a)), and by the end of the transmission band of design A2 at the other end (higher wavelength edge of shaded blue region in Fig. 3(b)).

Fig. 3(d) shows the calculated phase birefringence of design B

$$B_P = |n_y - n_x| \qquad (1)$$

as a function of wavelength. For the standard designs A1 and A2, as expected, the calculated phase birefringence is zero and both polarizations have identical confinement losses as a function of wavelength (overlapping in Fig. 3(a) and (b)). By contrast, in design B, there is a difference between the effective refractive indices of the two polarization modes resulting in the calculated phase birefringence in Fig. 3(d). There is also a clear difference in the calculated phase birefringence of design B in each transmission band with $B_P \sim 10^{-5}$ at 1550 nm – significantly higher than the birefringence in the short wavelength transmission band (in red). Correspondingly, there is a small difference in the calculated confinement loss for each polarization which is more noticeable towards the longer

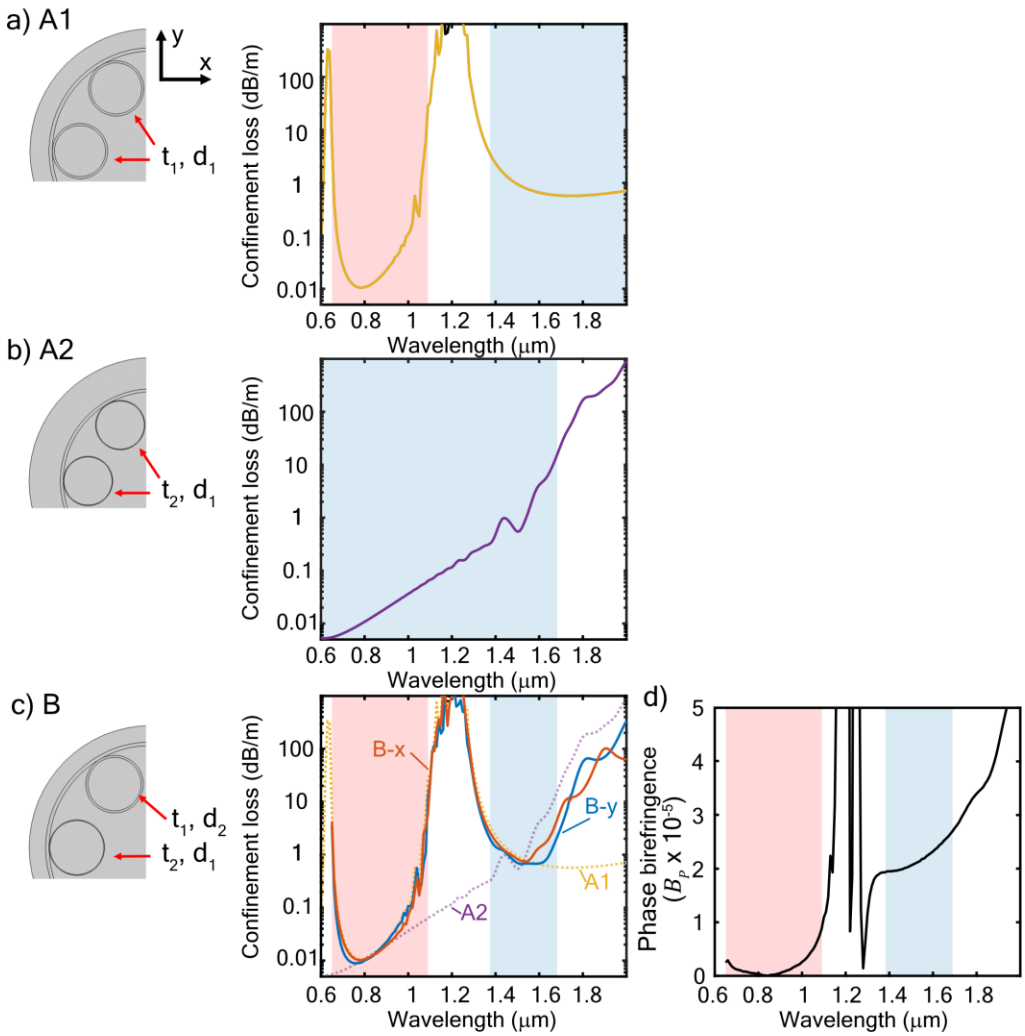

Fig. 3. Schematic diagram and calculated confinement loss (for the two orthogonal polarizations, *x* and *y*) of the simulated fiber based on (a) design A1, (b) design A2 and (c) design B. The calculated confinement loss for designs A1 and A2 is superimposed in dashed lines (as labelled) in (c) to guide the eye. The solid lines in (c) correspond to *x* and *y* of design B, respectively as indicated. (d) Calculated phase birefringence as a function of wavelength for design B. Blue/red shaded area highlights the longer/shorter wavelength anti-resonant transmission band.

wavelength range.

To explain the difference in the calculated phase birefringence in the two transmission bands of design B, we simulated the dependence of the birefringence on the core size of the structure. Figure 4 shows the simulations of the guidance properties of the fiber as a function of core size at 1550 nm. In these simulations, we modified the core size but kept the capillary tube thicknesses and the ratio between the core and capillary tube diameters fixed. As the core size decreases, corresponding to an increased interaction of the guided light with the surrounding glass structure, the calculated birefringence also increases. Nevertheless, this monotonic increase of the birefringence is accompanied by a steep increase in the confinement loss. This result is a clear illustration of the tradeoff between birefringence and loss in anti-resonant hollow-core fibers. The values for both the birefringence and the confinement loss of the fiber in design B (core size of 26 μm) are highlighted with dashed lines in Figure 4 as a guide to the eye.

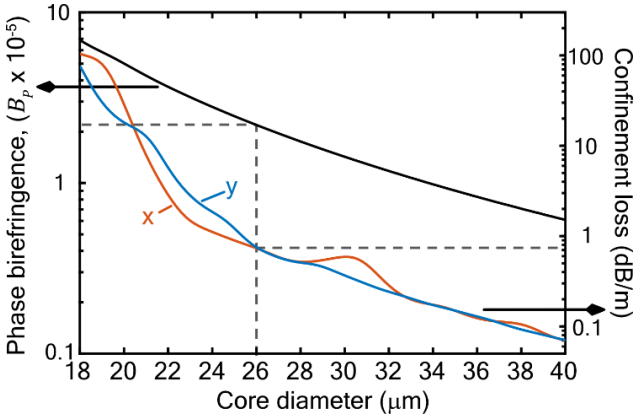

Fig. 4. Calculated phase birefringence and confinement loss (for n_x and n_y) at 1550 nm as a function of the core size of a fiber based on design B. For all core sizes, the capillary tube thicknesses are fixed at $t_1 = 610$ nm and $t_2 = 210$ nm, and the ratio between core and capillary tube diameters is set such that it is the same as in design B. Dashed lines indicate the corresponding phase birefringence and confinement loss for our fiber with core diameter 26 μm.

In addition, we simulated the confinement loss as a function of radius of the capillary tubes [24]. Interestingly, increasing

the radius of the capillary tubes and therefore decreasing the gaps between the capillary tubes increases the loss of the fiber. This is because in order to achieve the lowest confinement loss, the diameter of the air layer (inside the capillary tubes) must be at anti-resonance as well [22]. Simulating the phase birefringence and confinement loss as functions of core size at 800 nm shows a very weak dependence of phase birefringence on core size at this wavelength [24].

On the other hand, it is possible to achieve the same birefringence using a hollow core fiber with an elliptical core. We simulated such a fiber by taking a structure similar to design A1 and gradually increasing the ellipticity of the core. To achieve this, we increased the diameter of two capillary tubes (opposite to each other) while keeping the same thickness for all six capillary tubes ($t_1 = 610$ nm). Ellipticity of 1.5 was necessary in order to achieve birefringence of 2.7×10^{-5}. However, this comes with two main drawbacks: the fiber is no longer single mode, and the loss of the design increases rapidly with increasing ellipticity (4 dB/m for one orthogonal polarization, and 8 dB/m for the other). Similar behavior was observed when we increased the ellipticity of a fiber structure based on the capillary thickness t_2 of design A2.

III. Experimental Results

It is not trivial to measure the phase birefringence of our fiber with conventional methods like the sidescanning technique or the pinch roller method because the hollow core causes problems (e.g light scattering within the cladding, deformation of the hollow core, long beat length). However, our preliminary measurements with the sidescanning technique and with a cutback technique indicated the presence of a beat pattern which matches the anticipated beat length of ~ 6 cm.

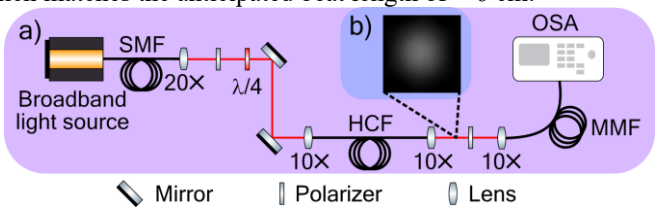

Fig. 5. (a) Experimental setup for measuring the fringe beat pattern of the two polarization states of the fiber. λ/4: quarter-wave plate, HCF: birefringent anti-resonant hollow-core fiber, MMF: multimode fiber, OSA: optical spectrum analyzer. (b) Near-field intensity pattern at the output of the fiber at 1550 nm.

On the other hand, it is possible to measure accurately the group birefringence [12]

$$B_G = B_P - \lambda \, {}^{dB}/_{d\lambda} \qquad (2)$$

of our fiber using the group beat length technique [25], [26]. For the beat length measurement, an SMF-28 patch cable was used to couple light from a broadband light source (near-IR edge-emitting LED source Agilent 83487a of spectral range 1100 nm -1600 nm) into a 10 m length of the hollow-core fiber, as shown in Fig. 5(a). As the light from the light source is unpolarized, a polarizer was introduced at the output of the light source. A broadband (1100 nm – 2000 nm) quarter-wave plate (Thorlabs, RABQ-1600) was also used to ensure that both polarization states of the hollow-core fiber are excited equally. At the output, a polarizer and an optical spectrum analyzer (OSA) were used to analyze the light from the hollow-core fiber. The output polarizer was set to ensure the strongest beat pattern resolved at the OSA. A near-IR camera (Xenics Xeva) and a 1550 nm laser diode (connected through the same fiber as the broadband light source) were also used to capture the near-field intensity pattern of the output of the fiber without disturbing the setup. The near-field intensity distribution (Fig. 5(b)) resembled a pure fundamental mode, suggesting the single mode performance of the fiber. By misaligning the input, we observed only a decrease in intensity, and no changes in the mode field profile of the output. This also indicates the single-mode performance of the fiber over a long enough length. Moreover, the simulated confinement loss of the higher order modes for design B was two orders of magnitude higher (~40 dB/m) than that of the fundamental mode [24].

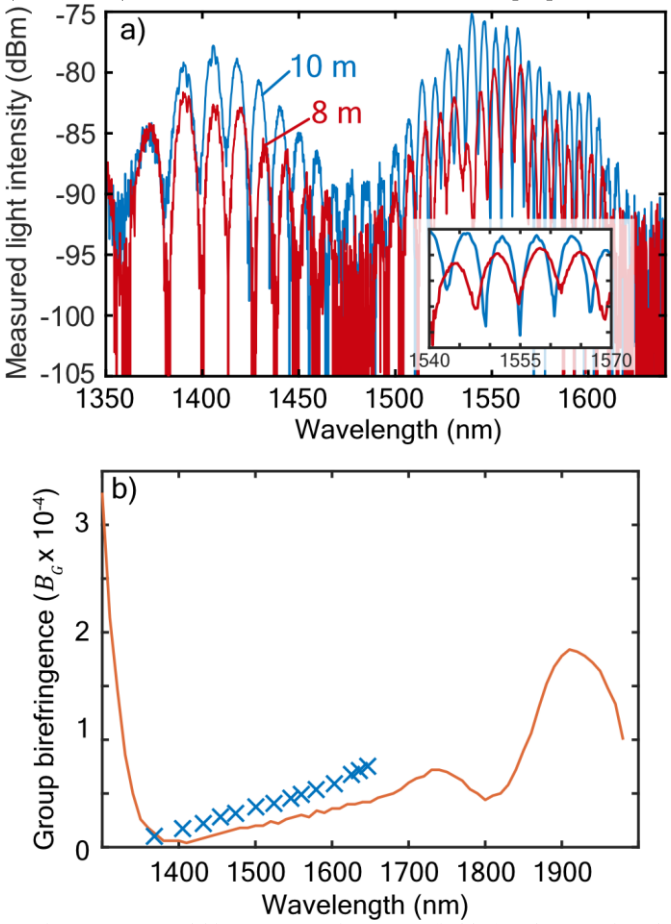

Fig. 6. (a) Spectral fringe pattern using a 10 m (in blue) and an 8 m (in red) piece of the birefringent hollow-core fiber. OSA resolution was 0.2 nm. Inset: Zoomed spectral fringe pattern showing fringe pattern for both lengths of fiber. (b) Simulated (orange line) and experimental (blue crosses) group birefringence as a function of wavelength.

Due to the birefringence of the fiber, the output light from the hollow-core fiber shows a strong characteristic spectral fringe pattern (Fig. 6(a)) when observed with the OSA. For a fiber of length L, the group birefringence (B_G) can be calculated using the spectral spacing of the fringes ($\Delta\lambda$) and equation:

$$B_G = \frac{\lambda_o^2}{L\Delta\lambda} \qquad (3)$$

with λ_o the central wavelength [6]. The fiber was cut down by two meters and the measurement repeated. As expected, the

fringe spectral spacing increased. In addition, rotating the quarter wave-plate affected the visibility of the fringes, confirming that the interference pattern is due to the birefringence of the fiber rather than to multimodal interference.

Using Equation 2 and the data for the simulated design B (with a two-point numerical differentiation method and smoothing), we obtained the group birefringence (Fig. 6(b), blue) for the range of wavelengths that we are interested in (between 1300 nm and 2000 nm). Fig. 6(b) also shows the experimental values of B_G calculated from the beat length measurement with Equation (1). The experimental and the simulated data follow the same trend, with a small offset in wavelength. This offset can be attributed to the accuracy of the capillary tube thicknesses that were measured from the SEM image in Fig. 2 and then used for the simulation (as per Table 1). Nevertheless, there is a clear correlation between the experimental and the simulated data. The measured magnitude of the group birefringence for the hollow-core fiber is $B_G = 4.4 \times 10^{-5}$ at 1550 nm, and the simulated value of the phase birefringence is around $B_P = 2.5 \times 10^{-5}$ at the same wavelength. In addition, when bending the fiber (around a 5 cm radius), the fringe pattern remained unchanged.

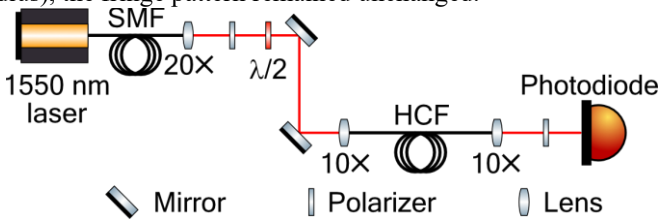

Fig. 7. Experimental setup for measuring the polarization extinction ratio. λ/2: half-wave plate, HCF: birefringent anti-resonant hollow-core fiber.

In addition, using the setup in Fig. 7 we measured the polarization extinction ratio (*PER*) of our fiber. Light from a 1550 nm laser was polarized with a polarizer and coupled into 5 m length of the birefringent hollow-core fiber. A half-wave plate was placed directly after the polarizer and rotated to excite only one of the two polarization modes of the fiber. Using a second polarizer and a photodiode detector at the output, we recorded the maximum and minimum voltage when rotating the output polarizer. The *PER* over a 5 m length of the fiber was calculated by

$$PER = 10\log\left(P_{max}/P_{min}\right), \quad (4)$$

where P_{max} and P_{min} are the respective maximum and minimum powers recorded when rotating the polarizer. We recorded a *PER* value of 23.1 dB for one polarization and 25.7 dB for the other. This corresponds to h-parameters of 9.8×10^{-4} and 5.3×10^{-4} for each polarization respectively. We also recorded the *PER* value of the setup without the fiber of 42.6 dB. In addition, bending the fiber around a radius of 5 cm resulted in no noticeable change in the position of P_{max} and P_{min}, as well as in the measured *PER*.

The cutback method was used to determine the transmission bands and the attenuation of the fabricated fiber of design B. White light from a Xe light source was coupled into the core of a 50 m length of the fiber and the transmission was recorded using an OSA. The fiber was cut back to 10 m and the transmission was recorded again. Fig. 8 shows the resulting attenuation spectrum of the fiber. We measured attenuation of 0.46 dB/m at 1550 nm. This measured loss is lower compared to the simulated loss at 1550 nm. We believe that the main reason for the discrepancy between measurement and simulation is due to the accuracy with which we can extract the thickness of the capillary tubes and the size of the core from the SEM image. We estimate a measurement error of at least 10% arising from the sharpness of the SEM image as well as the calibration accuracy of the machine. As shown in Fig. 4, a fiber with a 10% larger core will still have a phase birefringence of the order of 2×10^{-5}, but significantly lower confinement loss (0.45 dB/m) at 1550 nm. To further investigate the effect of our measurement uncertainty of the fiber geometry on the guidance properties of the fiber, we simulated different structures where we varied the capillary thicknesses by 5%. Doing so, we observed a significant change in the simulated loss (of about 30%), while the simulated phase birefringence showed only a 5% variation. We believe that lower loss can be achieved by fine tuning the thicknesses of the capillary tubes and the radii of the core and the capillary tubes.

In addition, based on our simulations we expect the fiber to present some amount of polarization dependent loss (PDL). Nevertheless, any PDL at 1550 nm must be low due to the fact that we were able to measure a clear group birefringence fringe pattern (10-20 dBm amplitude) across a 10 m length of fiber. Moreover, the *PER* measurement which was performed on each polarization axis of the fiber yielded very similar values (23.1 dB and 25.7 dB). This result is a further indication of the presence of a small amount of PDL.

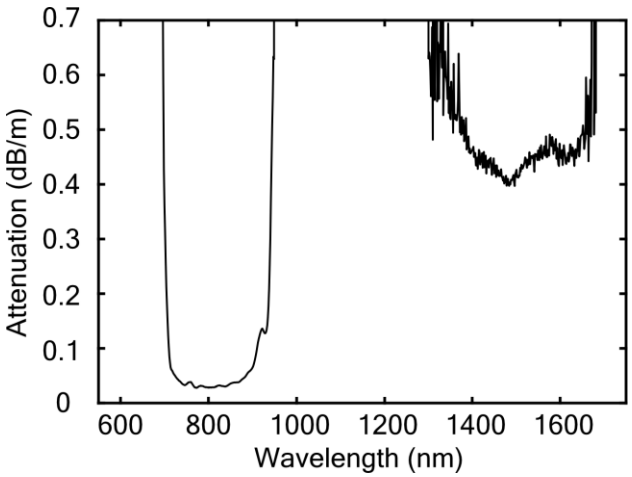

Fig. 8. Spectral attenuation of the birefringent hollow-core fiber.

IV. Conclusions

The calculated phase birefringence of our birefringent anti-resonant hollow-core fiber is two orders of magnitude lower compared to that of highly birefringent HC-PBGFs [12], [13], [25], and one order of magnitude lower compared to the phase birefringence of commercially available solid core polarization-maintaining fibers [11]. However, in HC-PBGFs the high birefringence is traded off for the narrow operational band and

complicated structure, making it a poor choice especially for broadband nonlinear processes [27]. On the other hand, the glass core of conventional solid-core polarization-maintaining fibers restricts their use in applications requiring pulsed light. Therefore, with its simple design, broadband operation, and air-guidance a birefringent anti-resonant hollow-core fiber is a significant leap forward.

To our knowledge, this is the first detailed demonstration of a birefringent anti-resonant hollow-core fiber. By using capillary tubes of two different thicknesses we achieved a phase birefringence of $\sim 10^{-5}$ at 1550 nm. Each set of capillary tubes has a guidance band at around 800 nm. We believe that the measured birefringent properties of this fiber at 1550 nm arise from the enhanced interaction of the guided light with the surrounding structure. At 1550 nm, the fiber operates at the lower edge of the first transmission band of the thicker capillary tubes and approaches the first resonance at ~1200 nm. Light guided at 1550 nm is also at the upper edge of the second transmission band (centered at 800 nm) of the thinner capillary tubes, where losses due to the small core size dominate [21]. Moreover, maintaining the loss of the fiber below 1 dB/m is crucial for the potential use of the fiber in various applications, such as polarization-maintaining fiber amplifiers [28] and sensing [29]. Stronger birefringence may be achieved [17], [18] by introducing a larger thickness or size dissimilarity between the capillary tubes. Lower loss may also be possible for larger core-sizes. However, the trade-off between attenuation loss and birefringence in hollow-core fibers is unavoidable.

Data underlying the results presented in the paper are available https://doi.org/10.15125/BATH-00767 [24].

ACKNOWLEDGMENT

We would like to thank Tim Birks, William Wadsworth, David Bird, James Stone and Peter Mosley for fruitful discussions.

FUNDING

We acknowledge support from the UK Engineering and Physical Sciences Research Council (EP/M013243/1, EP/K03197X/1 and EP/S001123/1) and Innovate UK project FEMTO-AAD (102671).

REFERENCES

[1] B. Debord *et al.*, "Multi-meter fiber-delivery and pulse self-compression of milli-Joule femtosecond laser and fiber-aided laser-micromachining," *Opt. Express*, vol. 22, no. 9, p. 10735, 2014.

[2] P. Jaworski, F. Yu, R. M. Carter, J. C. Knight, J. D. Shephard, and D. P. Hand, "High energy green nanosecond and picosecond pulse delivery through a negative curvature fiber for precision micro-machining," *Opt. Express*, vol. 23, no. 7, p. 8498, Apr. 2015.

[3] T. Frosch *et al.*, "Double antiresonant hollow core fiber – guidance in the deep ultraviolet by modified tunneling leaky modes," *Opt. Express*, vol. 22, no. 16, p. 19131, 2014.

[4] F. Yu, P. Song, D. Wu, T. Birks, D. Bird, and J. Knight, "Attenuation limit of silica-based hollow-core fiber at mid-IR wavelengths," *APL Photonics*, vol. 4, no. 8, p. 080803, Aug. 2019.

[5] G. Epple *et al.*, "Rydberg atoms in hollow-core photonic crystal fibres," *Nat. Commun.*, vol. 5, no. 1, p. 4132, Sep. 2014.

[6] S. Okaba *et al.*, "Lamb-Dicke spectroscopy of atoms in a hollow-core photonic crystal fibre," *Nat. Commun.*, vol. 5, no. 1, p. 4096, Sep. 2014.

[7] M. A. Terrel, M. J. F. Digonnet, and S. Fan, "Resonant fiber optic gyroscope using an air-core fiber," *J. Light. Technol.*, vol. 30, no. 7, pp. 931–937, 2012.

[8] B. Debord *et al.*, "Ultralow transmission loss in inhibited-coupling guiding hollow fibers," *Optica*, vol. 4, no. 2, p. 209, Feb. 2017.

[9] S. fei Gao *et al.*, "Hollow-core conjoined-tube negative-curvature fibre with ultralow loss," *Nat. Commun.*, vol. 9, no. 1, pp. 1–6, 2018.

[10] T. D. Bradley *et al.*, "Antiresonant Hollow Core Fibre with 0.65 dB/km Attenuation across the C and L Telecommunication Bands," *2019 Eur. Conf. Opt. Commun.*, vol. PD3.1, 2019.

[11] J. Noda, K. Okamoto, and Y. Sasaki, "Polarization-maintaining fibers and their applications," *J. Light. Technol.*, vol. 4, no. 8, pp. 1071–1089, 1986.

[12] M. S. Alam, K. Saitoh, and M. Koshiba, "High group birefringence in air-core photonic bandgap fibers," *Opt. Lett.*, vol. 30, no. 8, p. 824, Apr. 2005.

[13] J. M. Fini *et al.*, "Polarization maintaining single-mode low-loss hollow-core fibres," *Nat. Commun.*, vol. 5, no. 1, p. 5085, Dec. 2014.

[14] F. Yu and J. C. Knight, "Negative Curvature Hollow-Core Optical Fiber," *IEEE J. Sel. Top. Quantum Electron.*, vol. 22, no. 2, pp. 146–155, 2016.

[15] Y. Y. Wang, N. V. Wheeler, F. Couny, P. J. Roberts, and F. Benabid, "Low loss broadband transmission in hypocycloid-core Kagome hollow-core photonic crystal fiber," *Opt. Lett.*, vol. 36, no. 5, p. 669, Mar. 2011.

[16] A. D. Pryamikov, A. S. Biriukov, A. F. Kosolapov, V. G. Plotnichenko, S. L. Semjonov, and E. M. Dianov, "Demonstration of a waveguide regime for a silica hollow - core microstructured optical fiber with a negative curvature of the core boundary in the spectral region > 35 μm," *Opt. Express*, vol. 19, no. 2, p. 1441, Jan. 2011.

[17] S. A. Mousavi, S. R. Sandoghchi, D. J. Richardson, and F. Poletti, "Broadband high birefringence and polarizing hollow core antiresonant fibers," *Opt. Express*, vol. 24, no. 20, p. 22943, Oct. 2016.

[18] S. Yan, S. Lou, W. Zhang, and Z. Lian, "Single-polarization single-mode double-ring hollow-core anti-resonant fiber," *Opt. Express*, vol. 26, no. 24, p. 31160, Nov. 2018.

[19] S. Yan, S. Lou, X. Wang, T. Zhao, and W. Zhang, "High-birefringence hollow-core anti-resonant THz fiber," *Opt. Quantum Electron.*, vol. 50, no. 3, p. 162, Mar. 2018.

[20] W. Ding and Y.-Y. Wang, "Hybrid transmission bands and large birefringence in hollow-core anti-resonant fibers," *Opt. Express*, vol. 23, no. 16, p. 21165, Aug. 2015.

[21] D. Bird, "Attenuation of model hollow-core, anti-resonant fibres," *Opt. Express*, vol. 25, no. 19, p. 23215, 2017.

[22] P. Song, K. Y. Phoong, and D. Bird, "Quantitative analysis of anti-resonance in single-ring, hollow-core fibres," *Opt. Express*, vol. 27, no. 20, p. 27745, Sep. 2019.

[23] P. Uebel *et al.*, "Broadband robustly single-mode hollow-core PCF by resonant filtering of higher-order modes," *Opt. Lett.*, vol. 41, no. 9, p. 1961, May 2016.

[24] S. Yerolatsitis, R. Shurvinton, P. Song, Y. Zhang, R. J. A. Francis-Jones, and K. R. Rusimova, "Dataset for Birefringent Anti-resonant Hollow-core Fiber." Bath: University of Bath Research Data Archive. https://doi.org/10.15125/BATH-00767.

[25] X. Chen *et al.*, "Highly birefringent hollow-core photonic bandgap fiber," *Opt. Express*, vol. 12, no. 16, p. 3888, 2004.

[26] S. Yerolatsitis, R. Shurvinton, P. Song, R. J. A. Francis-Jones, and K. R. Rusimova, "Birefringent anti-resonant hollow-core fibre," *Proc. Eur. Conf. Opt. Commun.*, vol. Tu2E3, 2019.

[27] P. S. J. Russell, P. Hölzer, W. Chang, A. Abdolvand, and J. C. Travers, "Hollow-core photonic crystal fibres for gas-based nonlinear optics," *Nat. Photonics*, vol. 8, no. 4, pp. 278–286, Apr. 2014.

[28] X. Peng and L. Dong, "Fundamental-mode operation in polarization-maintaining ytterbium-doped fiber with an effective area of 1400 μm^2," *Opt. Lett.*, vol. 32, no. 4, p. 358, 2007.

[29] N. Gayraud *et al.*, "Mid-infrared gas sensing using a photonic bandgap fiber," *Appl. Opt.*, vol. 47, no. 9, p. 1269, Mar. 2008.